Thomas-Fermi screening of electrostatic fields in a type-I superconductor

Nikhil Seeja Sivakumar, Tyler James, Frederick Carlisle, Philip Moriarty, and Brian Kiraly*
School of Physics and Astronomy, University of Nottingham, Nottingham NG7 2RD, United Kingdom

(Received 6 September 2026; accepted 20 October 2026; published 17 November 2026)

The empirical London equations make distinct predictions for a superconductor's longitudinal and transverse electrodynamic response. Conventionally, this framework attributes the Meissner effect to the transverse component, with the longitudinal response predicted to remain unchanged upon entering the superconducting state, i.e., a static electric field is screened over the Thomas-Fermi length ($\lambda_{TF} \sim 1$ Å), just as in the nonsuperconducting metal. Hirsch [Phys. Rev. B **69**, 214515 (2004)] has developed an alternative formalism, which predicts that the longitudinal screening length should instead be governed by the London penetration depth as the system is cooled below the superconducting transition temperature (T_c). Here, we use a combination of qPlus atomic force microscopy and scanning tunneling microscopy/spectroscopy of single-crystal Pb(111) at ∼340 mK ($T/T_c \sim 0.05$) in an attempt to detect any modifications in electrostatic screening of the longitudinal tip field upon entering the superconducting phase. We quench superconductivity using a magnetic field of 200 mT normal to the Pb(111) surface. By measuring force-distance curves and local field-emission resonance spectra at the same sample position in the presence and absence of the magnetic field, we constrain the change in screening between the normal and superconducting state to less than ∼1%. This is between two to three orders of magnitude smaller than that predicted by Hirsch's theory, and entirely consistent with unmodified Thomas-Fermi screening across the superconducting transition.

DOI: 10.1103/9x2v-9sb1

I. INTRODUCTION

The electrodynamic response of a superconductor (SC) has been debated since the London formulation was first put forward almost a century ago [1]. In traditional BCS theory, the SC order parameter has both an amplitude and phase, and the latter must be treated in concert with the vector potential to realize a fully gauge-invariant formulation of SC electrodynamics [2–4]. The conventional approach attributes magnetic field screening to the transverse electromagnetic response over length scales of the London penetration depth (λ_L)—thereby producing the Meissner effect—whereas the static longitudinal response screens electric fields over the much shorter Thomas-Fermi screening length (λ_{TF}). Hirsch has instead argued, through a series of occasionally provocative papers [5–10], that the invariance requirement is more naturally satisfied in the Lorenz gauge, under which the SC wave function is equally rigid against electric and magnetic perturbations, so that the natural screening length for *both* **E** and **B** fields is λ_L. Consequently, the static electrostatic screening length constitutes a direct experimental discriminant between these competing descriptions of the SC state. Beyond its significance for the foundations of SC, resolving this question is of particular relevance for emerging SC technologies, including electrostatically controlled SC devices [11,12], SC field-effect transistors [13,14], and atomically thin SC [15–18]. Descriptions of electrostatic control in these systems combine screening with changes in carrier density [15] and confinement-dependent modifications of the balance between electron-phonon attraction and effective Coulomb repulsion [17,18].

Most experimental studies infer screening properties nonlocally in capacitive geometries [19,20] or indirectly through measurements of microwave surface impedance [21–24], or optical/terahertz conductivity [25–27] rather than through direct probes of static electric-field screening. In contrast, a local probe is uniquely capable of measuring the spatial dependence of the electrostatic interaction itself, providing direct access to the screening response of the condensate and disentangling screening from alternative coexisting surface signals. Recognizing this, Hirsch proposed a scanning probe experiment designed to detect the predicted modification of electrostatic screening in the SC state [8]. Peronio and Giessibl [28] elegantly adapted that proposal to a qPlus atomic force microscope (AFM) to measure the electrostatic interaction between the Smoluchowski dipole [29] at the probe apex and a Nb(110) surface, searching for signatures of the predicted change in screening length. While their experiments established an important benchmark, the achievable force sensitivity prevented a definitive determination of the screening response, leaving the question unresolved.

Here, we overcome these limitations by combining the force sensitivity of a cryogenic qPlus sensor with the local spectroscopic capabilities of the scanning tunneling microscope (STM) (via field-emission resonances [30–34]), enabling a direct real-space measurement of the electrostatic

*Contact author: brian.kiraly@nottingham.ac.uk

Published by the American Physical Society under the terms of the Creative Commons Attribution 4.0 International license. Further distribution of this work must maintain attribution to the author(s) and the published article's title, journal citation, and DOI.

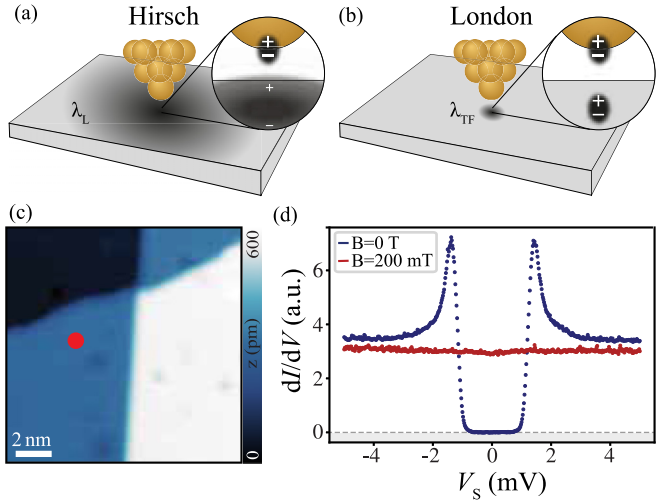


FIG. 1. Sketch showing the screening of the tip dipole by the superconductor in the case of (a) Hirsch's alternative theory [5] (screening length $\sim\lambda_L$, the London penetration depth) and (b) traditional London (BCS) theory (Thomas-Fermi screening length, λ_{TF}). (c) STM image of Pb(111) surface ($V_S = 100$ mV; $I_t = 100$ pA). (d) dI/dV spectra measured in the presence (red) and absence (blue) of a 200 mT magnetic field applied normal to the Pb(111) sample surface. Stabilization parameters: $V_S = 5$ mV; $I_t = 100$ pA; lock-in amplifier modulation amplitude =20 μV.

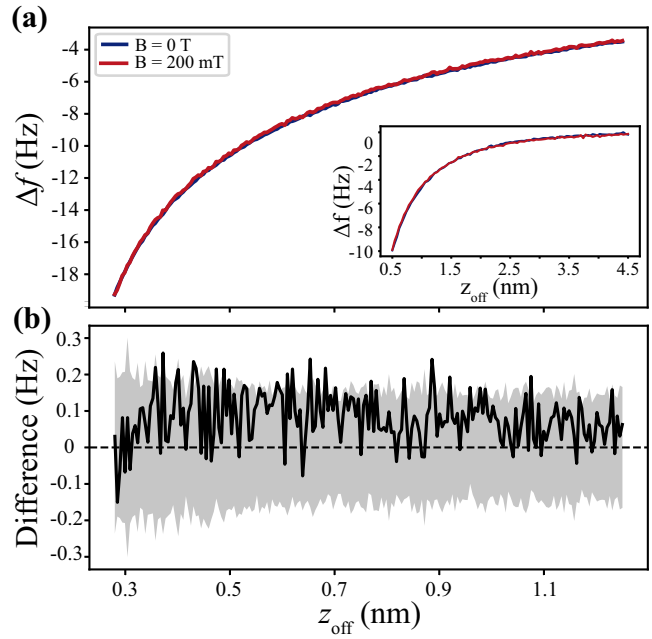


FIG. 2. (a) Averaged set of $\Delta f(z)$ measurements on the Pb(111) surface with $B = 0$ T (blue, $N = 60$ curves) and $B = 200$ mT (red, $N = 24$), respectively. Inset: Similar measurement over a much larger z range. (b) Difference signal between $B = 0$ T and $B = 200$ mT, with the shaded region given by the 99% confidence interval associated with the pooled standard error. Stabilization parameters: $V_S = 5$ mV, $I_t = 100$ pA, oscillation amplitude = 100 pm.

screening response of the SC condensate. To provide the clearest possible discrimination, we operate at approximately 340 mK, where $T/T_c \sim 0.05$ and $\lambda_L \sim 53$ nm, and we quench SC with a magnetic field (Fig. 1) rather than a temperature ramp [28]. The combined effect is to dramatically reduce measurement uncertainty while simultaneously enhancing the magnitude of the effective observable: Hirsch's prediction corresponds to three orders of magnitude difference in the screening ($\lambda_L/\lambda_{TF} \sim 10^3$) for bulk Pb [35].

II. RESULTS

We focus on screening of the Smoluchowski dipole at the apex of the scanning probe [28] by the underlying Pb(111) surface [sketched schematically in Figs. 1(a) and 1(b)]. For our purposes, a perfect metal is represented by the presence of an image dipole whose magnitude and position are exactly equal and opposite that of the tip [Fig. 1(b)]. The presence of imperfect screening [Fig. 1(a)] instead causes the voltage to be dropped over a volume inside the sample—as for semiconductors where the Fermi level can respond to the tip-induced field [36]—reducing the magnitude of the effective image dipole at the tunnel junction.

Following sputter annealing, an atomically flat Pb(111) surface was obtained [Fig. 1(c)]. (See Supplemental Material [37] for detailed information on sample preparation and measurement protocols.) In the absence of a magnetic field, the SC gap of the Pb(111) surface is well resolved in dI/dV spectra [Fig. 1(d), spectrum in blue]. Throughout our experiments, care was taken to ensure that the differential conductance spectra were also free of any indication of an additional SC gap that might arise from appreciable quantities of lead adsorbed on the tip. Application of a magnetic field of 200 mT normal to the sample surface quenches the sample SC, as evidenced by the removal of the characteristic gap around the Fermi level in the dI/dV spectrum [Fig. 1(d), spectrum in red]. The presence of fiducial surface features such as surface defects and step edges ensure that the tip can be reliably and reproducibly repositioned.

A. Non-contact atomic force microscopy

In the first set of experiments, we followed the methodology introduced by Peronio and Giessibl [28]: frequency shift versus tip sample separation [$\Delta f(z)$] curves measured at the same position on the Pb(111) surface are used to determine whether there are changes in the force gradient experienced by the qPlus tuning fork sensor in the superconducting versus normal states. Averaged $\Delta f(z)$ curves acquired at the position denoted by the red dot in Fig. 1(c) are shown in Fig. 2(a). All sets of measurements were made at the same lateral position (to a precision of better than 1 Å) and with identical initial feedback/stabilization parameters far from the superconducting gap onset to set the starting tip height (i.e., the initial z value). The z data are then offset by setting $z = 0$ when $G = G_0$ upon extrapolation of $I - z$ curves (Fig. S2 [37]). The set-point oscillation amplitude of 100 pm was controlled to better than 2% for the duration of the z ramp (Fig. S1 [37]), and, in line with Peronio and Giessibl's measurement strategy [28], a sample voltage of 70 μV (compensating the overall offset bias in the control electronics) was used to minimize the tunneling current. The $\Delta f(z)$ curves were repeated over multiple individual measurements to both improve accuracy

and, as described in detail below, derive statistical uncertainties; the average of all $B = 0$ T (blue) and $B = 200$ mT (red) curves are shown in Fig. 2(a). The inset shows a similar averaged $\Delta f(z)$ curve, acquired over a larger z range. During the frequency-shift measurements, the presence of the superconducting phase was routinely confirmed via scanning tunneling spectroscopy.

To place a rigorous bound on any magnetic-field-induced change in the $\Delta f(z)$ curves, we first calculate the mean and variance for the sets of "field" (B) and "no-field" ($B = 0$) measurements: $\langle \Delta f \rangle_B(z)$, $\sigma_B^2(z)$, $\langle \Delta f \rangle_{B=0}(z)$, and $\sigma_{B=0}^2(z)$, where $\langle\,\rangle$ denotes the mean, and σ^2 the variance. The combined standard error of the difference between these two sets is then

$$\mathcal{E}(z) = \sqrt{\frac{\sigma_B^2(z)}{n_B} + \frac{\sigma_{B=0}^2(z)}{n_{B=0}}}, \tag{1}$$

where σ^2 is the variance and n_B, $n_{B=0}$ are the number of $\Delta f(z)$ curves in the field and no-field sets, respectively. We calculate the difference between the two mean curves, $\langle \Delta f \rangle_{B=0}(z) - \langle \Delta f \rangle_B(z)$ [black line, Fig. 2(b)], and compare to the 99% confidence interval (CI) derived from $\mathcal{E}(z)$ [shaded region, Fig. 2(b)]. The measured difference lies predominantly within this CI, indicating that it is consistently below the threshold of experimental uncertainty. A root-mean-square (rms) value for the difference over the entire curve in Fig. 2(b), $D_{\text{rms}} = 0.11$ Hz, is likewise well below the total rms uncertainty of 0.17 Hz. Our results therefore indicate, at a 99% confidence level, that any superconductivity-induced change in the measured force-gradient curve must be smaller than 0.17 Hz rms over the investigated distance range. If we use the simple dipole-dipole interaction model (Fig. S3 [37]) suggested by Peronio and Giessibl [28], this result constrains the upper limit on the change in the image dipole to 0.01 D.

B. Field emission resonance spectroscopy

As an independent measurement of possible variation in electrostatic screening at the tip-sample junction, we turn to field-emission resonance (FER) spectroscopy [30–32]. FERs arise when electrons tunneling from the tip become transiently trapped in quasibound states within the potential well bounded by the sample surface barrier and the tip [30,31]. This well is formed by the combination of the image potential at the sample surface and the applied electric field; the former contributes significantly at low energies, while at sufficiently high positive sample bias the latter dominates, giving rise to a discrete ladder of quasi-triangular-well states—essentially Gundlach oscillations [33]—observed as a series of resonances in dI/dV (or dz/dV) spectra in the field-emission regime [31–34]. As such, the energies of the FER states are highly sensitive to the local electrostatic environment and have accordingly been used to map local work-function variations with high spatial resolution [32–34]. Field-emission resonance spectroscopy is therefore particularly well suited to testing whether electrostatic screening changes between the superconducting and normal states of Pb(111).

FER spectra (Fig. 3) were acquired in constant-current mode [31], with dI/dV spectra of the superconducting gap, alongside $\Delta f(z)$ and $I(z)$ curves, checked frequently between measurements to ensure that the tip state was preserved throughout. Figure 3(a) shows a set of resonances for sample biases in the +3 to +8 V range in the superconducting (blue) and normal (red) states. The FER spectra lie atop one another with no observable differences at this scale, including measurements made with varying tip apices (Fig. S6 [37]). To establish a quantitative bound on this result, we restrict our analysis to the $n = 1, 2, 3$ FERs. Each individual resonance was fit with a Lorentzian peak to extract its peak center; an example for the $n = 2$ resonance is shown in Fig. 3(b). Pure Lorentzian fits were robust over a range of ±200 mV around each peak center, V_p, despite some asymmetry related to the spectral background often seen in tunneling spectroscopy. Repeated measurements under field and no-field conditions are shown in Fig. 3(c). For each resonance, we compare the peak position of an individual measurement, $V_{p,n}$, to the group average, $\langle V_{p,n} \rangle$; pooling this deviation across $n = 1, 2, 3$ yields the histograms shown. The field (red) and no-field (blue) distributions entirely overlap, each with a mean difference of 0.0 mV and a 99% confidence interval of ±0.5 mV. The FER results are therefore entirely consistent with the force-gradient measurements of Fig. 2, confirming that the electrostatic response of the sample is indistinguishable between the superconducting and normal states. Any superconductivity-induced shift in the FER peak positions must be smaller than our experimental bound of 0.5 meV. We next convert this limit into a constraint on the magnitude of the image dipole.

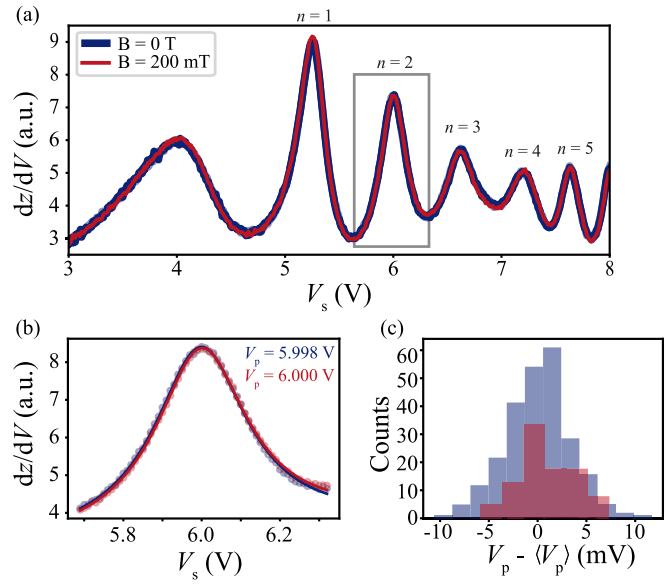


FIG. 3. (a) Constant-current dz/dV spectrum as a function of applied bias in the field-emission regime for no magnetic field (blue) and an applied B field of 200 mT normal to the Pb(111) surface. (b) $n = 2$ field-emission resonance for both the zero-field (blue) and applied field (red) conditions, with Lorentzian fits (solid lines). (c) Histogram of the deviation of each measured FER peak position from its resonance-specific mean, pooled over $n = 1, 2, 3$ and separated by field (red) and no-field (blue) conditions.

In order to relate the 0.5 meV bound on shifts in the FER resonances to the local electrostatic response of the tip-sample junction, we constructed a model one-dimensional potential and solved the Schrödinger equation to find the

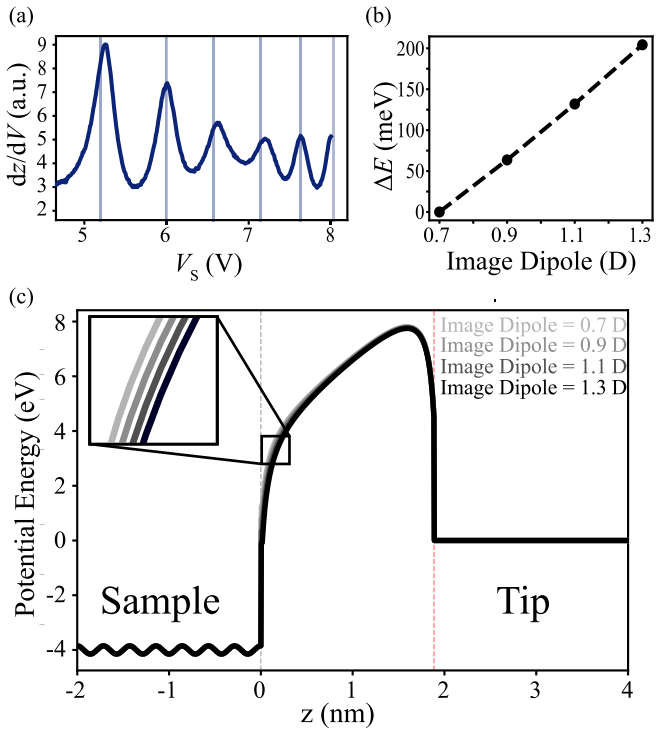


FIG. 4. (a) Comparison of experimentally measured peak positions of field-emission resonances (blue line, no magnetic field) with those predicted by the simple model described in the text (vertical light blue lines, see also Supplemental Material [37]). (b) Predicted shift in resonance energy as a function of the magnitude of the image dipole. (c) Electrostatic potential used in the simulations; the inset shows the influence of the image dipole on the form of the potential.

characteristic energy eigenstates inside the vacuum region (Fig. 4), following the approach of Ploigt *et al.* [32]. The potential used in the simulations is shown in Fig. 4(c): The Pb(111) crystal is modeled with a small periodic potential commensurate with the Pb lattice constant. A small number of physically motivated parameters—the tip and image dipole moments, together with the sample work function and tip-sample separation—are sufficient to account for the spectrum of observed FER energies [light blue lines, Fig. 4(a)], giving us confidence in the model's ability to adequately capture the underlying electrostatics. As a further test of the model's sensitivity to changes in the electrostatic energy landscape, we compared FER spectra measured on the Pb(111) terrace and at a step edge, the latter known to host a Smoluchowski dipole [29,40]; the model reproduces the difference between the two spectra well, accounting for it with only a small change in the sample dipole moment (see Fig. S5 [37]). We then translate the 0.5 meV bound on the resonance energy shift into a constraint on the image dipole: Tuning the dipole moment and tracking the resulting shift in the simulated FER peak energies [Fig. 4(b)] gives a sensitivity of approximately 350 mV/D. This in turn constrains any superconductivity-induced change in the image dipole to less than 0.001 D, an order of magnitude tighter than the 0.01 D bound obtained from the force-based $\Delta f(z)$ measurements.

III. CONCLUSIONS

In summary, the techniques employed here probe the electrostatic response of the superconducting condensate through entirely different physical channels—one via the force gradient for a scanning probe, the other via the energy of quasibound electronic states in the tunnel junction—yet arrive at the same conclusion: the image dipole at the tip-sample junction is unaffected, within tight experimental bounds (99% confidence intervals), by the onset of superconductivity. Our results reaffirm that the Meissner effect is a purely transverse phenomenon, with no accompanying change in the superconductor's response to static electric fields. More broadly, this work demonstrates the sensitivity that combined force- and spectroscopy-based scanning probe techniques bring to the electrostatics of the superconducting state, an approach that could be extended to electrostatically gated systems and unconventional superconductors [41,42].

ACKNOWLEDGMENTS

We gratefully acknowledge technical assistance from Nick Botterill and Yutaka Miyatake. This work was supported by the Engineering and Physical Sciences Research Council, Grant Reference No. EP/Y023250/1. P.M. thanks the EPSRC for support from the award of an Established Career Fellowship (EP/T033568/1).

DATA AVAILABILITY

All raw data from this work are available at the University of Nottingham Research Data Management Repository [43].

[1] F. London and H. London, The electromagnetic equations of the supraconductor, Proc. R. Soc. A **149**, 71 (1935)
[2] P. W. Anderson, Random-phase approximation in the theory of superconductivity, Phys. Rev. **112**, 1900 (1958).
[3] Y. Nambu, Quasi-particles and gauge invariance in the theory of superconductivity, Phys. Rev. **117**, 648 (1960).
[4] T. Koyama, Comment on "Charge expulsion and electric field in superconductors", Phys. Rev. B **70**, 226503 (2004).
[5] J. E. Hirsch, Charge expulsion and electric field in superconductors, Phys. Rev. B **68**, 184502 (2003).
[6] J. E. Hirsch, Electrodynamics of superconductors, Phys. Rev. B **69**, 214515 (2004).
[7] J. E. Hirsch, Experimental consequences of predicted charge rigidity of superconductors, Phys. C: Supercond. **478**, 42 (2012).
[8] J. E. Hirsch, Proposed experimental test of an alternative electrodynamic theory of superconductors, Phys. C: Supercond. Appl. **508**, 21 (2015).
[9] J. E. Hirsch, *Superconductivity Begins with H, Both Properly Understood and Misunderstood: Superconductivity Basics Rethought* (World Scientific, Singapore, 2020).
[10] J. E. Hirsch, Reply to "Comment on 'Charge expulsion and electric field in superconductors"', Phys. Rev. B **70**, 226504 (2004).

[11] A. E. Antipov, A. Bargerbos, G. W. Winkler, B. Bauer, E. Rossi, and R. M. Lutchyn, Effects of gate-induced electric fields on semiconductor Majorana nanowires, Phys. Rev. X **8**, 031041 (2018).

[12] J. Chen, P. Yu, J. Stenger, M. Hocevar, D. Car, S. R. Plissard, E. P. A. M. Bakkers, T. D. Stanescu, and S. M. Frolov, Experimental phase diagram of zero-bias conductance peaks in superconductor/semiconductor nanowire devices, Sci. Adv. **3**, e1701476 (2017).

[13] G. De Simoni, F. Paolucci, P. Solinas, E. Strambini, and F. Giazotto, Metallic supercurrent field-effect transistor, Nat. Nanotechnol. **13**, 802 (2018).

[14] F. Paolucci, F. Crisá, G. De Simoni, L. Bours, C. Puglia, E. Strambini, S. Roddaro, and F. Giazotto, Electrostatic field-driven supercurrent suppression in ionic-gated metallic superconducting nanotransistors, Nano Lett. **21**, 10309 (2021).

[15] J. T. Ye, Y. J. Zhang, R. Akashi, M. S. Bahramy, R. Arita, and Y. Iwasa, Superconducting dome in a gate-tuned band insulator, Science **338**, 1193 (2012).

[16] Y. Saito, Y. Kasahara, J. Ye, Y. Iwasa, and T. Nojima, Metallic ground state in an ion-gated two-dimensional superconductor, Science **350**, 409 (2015).

[17] A. Zaccone and V. M. Fomin, Theory of superconductivity in thin films under an external electric field, Phys. Rev. B **109**, 144520 (2024).

[18] A. Zaccone, G. A. Ummarino, A. Braggio, and F. Giazotto, Microscopic mechanism of electric-field-induced superconductivity suppression in metallic thin films, Phys. Rev. B **111**, 174528 (2025).

[19] H. London, An experimental examination of the electrostatic behaviour of supraconductors, Proc. R. Soc. A **155**, 102 (1936).

[20] R. E. Glover and M. D. Sherrill, Changes in superconducting critical temperature produced by electrostatic charging, Phys. Rev. Lett. **5**, 248 (1960).

[21] D. C. Mattis and J. Bardeen, Theory of the anomalous skin effect in normal and superconducting metals, Phys. Rev. **111**, 412 (1958).

[22] J. Halbritter, Surface residual resistance of high-Q-superconducting resonators, J. Appl. Phys. **42**, 82 (1971).

[23] J. P. Turneaure and I. Weissman, Microwave surface resistance of superconducting niobium, J. Appl. Phys. **39**, 4417 (1968).

[24] T. Junginger, S. Aull, W. Weingarten, and C. P. Welsch, Experimental evidence for electric surface resistance in niobium, IEEE Trans. Appl. Supercond. **27**, 3500607 (2017).

[25] R. E. Glover and M. Tinkham, Conductivity of superconducting films for photon energies between 0.3 and $40kT_c$, Phys. Rev. **108**, 243 (1957).

[26] U. S. Pracht, E. Heintze, C. Clauss, D. Hafner, R. Bek, D. Werner, S. Gelhorn, M. Scheffler, M. Dressel, D. Sherman, B. Gorshunov, K. S. Il'n, D. Henrich, and M. Siegel, Electrodynamics of the superconducting state in ultra-thin films at THz frequencies, IEEE Trans. Terahertz Sci. Technol. **3**, 269 (2013).

[27] K. I. Sim, Y. C. Jo, T. Ha, J. H. Kim, J. H. Kim, and H. Yamamori, Terahertz electrodynamics and superconducting energy gap of NbN, J. Korean Phys. Soc. **71**, 571 (2017).

[28] A. Peronio and F. J. Giessibl, Attempts to test an alternative electrodynamic theory of superconductors by low-temperature scanning tunneling and atomic force microscopy, Phys. Rev. B **94**, 094503 (2016).

[29] R. Smoluchowski, Anisotropy of the electronic work function of metals, Phys. Rev. **60**, 661 (1941).

[30] R. S. Becker, J. A. Golovchenko, and B. S. Swartzentruber, Electron interferometry at crystal surfaces, Phys. Rev. Lett. **55**, 987 (1985).

[31] G. Binnig, K. H. Frank, H. Fuchs, N. Garcia, B. Reihl, H. Rohrer, F. Salvan, and A. R. Williams, Tunneling spectroscopy and inverse photoemission: Image and field states, Phys. Rev. Lett. **55**, 991 (1985).

[32] H.-C. Ploigt, C. Brun, M. Pivetta, F. Patthey, and W.-D. Schneider, Local work function changes determined by field emission resonances: NaCl/Ag(100), Phys. Rev. B **76**, 195404 (2007).

[33] C. L. Lin, S. M. Lu, W. B. Su, H. T. Shih, B. F. Wu, Y. D. Yao, C. S. Chang, and T. T. Tsong, Manifestation of work function difference in high order Gundlach oscillation, Phys. Rev. Lett. **99**, 216103 (2007).

[34] A. Y. Aladyshkin, Quantum-well and modified image-potential states in thin Pb(111) films: An estimate for the local work function, J. Phys.: Condens. Matter **32**, 435001 (2020).

[35] R. D. Muiño, D. Sánchez-Portal, V. M. Silkin, E. V. Chulkov, and P. M. Echenique, Time-dependent electron phenomena at surfaces, Proc. Natl. Acad. Sci. USA **108**, 971 (2011).

[36] M. Weimer, J. Kramar, and J. D. Baldeschwieler, Band bending and the apparent barrier height in scanning tunneling microscopy, Phys. Rev. B **39**, 5572(R) (1989).

[37] See Supplemental material at http://link.aps.org/supplemental/10.1103/9x2v-9sb1 for details of the experimental methods, force distance measurement protocol, absolute tip sample distance calibration, dipole-interaction model, magnetic-field control measurements on Ag(111), field-emission-resonance measurements at Pb(111) step edges, and reproducibility measurements using multiple tip apices, which includes Refs. [38,39].

[38] J. Y. Park, G. M. Sacha, M. Enachescu, D. F. Ogletree, R. A. Ribeiro, P. C. Canfield, C. J. Jenks, P. A. Thiel, J. J. Sáenz, and M. Salmeron, Sensing dipole fields at atomic steps with combined scanning tunneling and force microscopy, Phys. Rev. Lett. **95**, 136802 (2005).

[39] J. F. Jia, K. Inoue, Y. Hasegawa, W. S. Yang, and T. Sakurai, Variation of the local work function at steps on metal surfaces studied with STM, Phys. Rev. B **58**, 1193 (1998).

[40] D. Yu, H. P. Bonzel, and M. Scheffler, Orientation-dependent surface and step energies of Pb from first principles, Phys. Rev. B **74**, 115408 (2006).

[41] Y. Cao, V. Fatemi, S. Fang, K. Watanabe, T. Taniguchi, E. Kaxiras, and P. Jarillo-Herrero, Unconventional superconductivity in magic-angle graphene superlattices, Nature (London) **556**, 43 (2018).

[42] M. Oh, K. P. Nuckolls, D. Wong, R. L. Lee, X. Liu, K. Watanabe, T. Taniguchi, and A. Yazdani, Evidence for unconventional superconductivity in twisted bilayer graphene, Nature (London) **600**, 240 (2021).

[43] University of Nottingham Research Data Management Repository, https://doi.org/10.17639/nott.39715.